B-T-3288

# STRESS INTENSITY FACTOR PLASTICITY CORRECTION FOR FLAWS IN STRESS CONCENTRATION REGIONS

E. Friedman
W. K. Wilson



DE-AC11-98PN38206



BETTIS ATOMIC POWER LABORATORY WEST MIFFLIN, PENNSYLVANIA 15122-0079

Operated for the U.S. Department of Energy
by Bechtel Bettis, Inc.

## DISCLAIMER

## DISCLAIMER

Portions of this document may be illegible in electronic image products. Images are produced from the best available original document.

# STRESS INTENSITY FACTOR PLASTICITY CORRECTION FOR FLAWS IN STRESS CONCENTRATION REGIONS

**Edward Friedman**
**William K. Wilson**

Bechtel Bettis, Inc.
Bettis Atomic Power Laboratory
West Mifflin, PA

## ABSTRACT

Plasticity corrections to elastically computed stress intensity factors are often included in brittle fracture evaluation procedures. These corrections are based on the existence of a plastic zone in the vicinity of the crack tip. Such a plastic zone correction is included in the flaw evaluation procedure of Appendix A to Section XI of the ASME Boiler and Pressure Vessel Code. Plasticity effects from the results of elastic and elastic-plastic explicit flaw finite element analyses are examined for various size cracks emanating from the root of a notch in a panel and for cracks located at fillet radii. The results of these calculations provide conditions under which the crack-tip plastic zone correction based on the Irwin plastic zone size overestimates the plasticity effect for crack-like flaws embedded in stress concentration regions in which the elastically computed stress exceeds the yield strength of the material. A failure assessment diagram (FAD) curve is employed to graphically characterize the effect of plasticity on the crack driving force. The Option 1 FAD curve of the Level 3 advanced fracture assessment procedure of British Standard PD 6493:1991, adjusted for stress concentration effects by a term that is a function of the applied load and the ratio of the local radius of curvature at the flaw location to the flaw depth, provides a satisfactory bound to all the FAD curves derived from the explicit flaw finite element calculations. The adjusted FAD curve is a less restrictive plasticity correction than the plastic zone correction of Section XI for flaws embedded in plastic zones at geometric stress concentrators. This enables unnecessary conservatism to be removed from flaw evaluation procedures that utilize plasticity corrections.

## INTRODUCTION

Brittle fracture evaluation procedures as given, for example, in Section XI of the ASME Boiler and Pressure Vessel Code (ASME, 1998) or the British Standard PD 6493, 1991 use linear elastic stress intensity factors for crack configurations in simple geometries to characterize the crack driving force for crack-like flaws located in regions of more complex geometry. In particular, the stress intensity factor solutions applied to surface flaws in such geometries are often those for surface cracks in finite thickness flat plates or in cylindrical shells. This approach is often called the implicit method since the stress intensity factor is determined implicitly from (1) the stress distribution existing at the crack location but calculated in the absence of the crack, and (2) a stress intensity factor solution for a structure whose geometry may not resemble that of the region in which the crack is located. An example of this is a stress concentration region such as a notch or a fillet radius. The stress intensity factor calculation directly accounts for neither the geometry of the structure nor the source or nature of the loading that drives the crack. Explicit procedures such as energy release rate or domain integral methods that utilize finite element models with cracks included explicitly in the model accommodate the interaction of the crack, the component geometry, and the loading. This interaction can be especially important when distinguishing between cracks driven by primary loading, such as pressure, and secondary loading, such as thermal or residual stresses.

The effects of plasticity in flaw evaluation procedures are often expressed in terms of a plastic zone correction factor (see, for example, ASME, 1998) which is predicated on the assumption that the flaw is located in a region whose behavior is elastic if the flaw did not exist. Furthermore, in the presence of the crack-like flaw, a plastic zone existing in the vicinity of the crack tip simulates the plasticity effect. The size of the plastic zone is presumed to be small relative to the crack size or any other characteristic dimension. An effective crack size is then defined as the sum of the actual crack size and the distance from the crack tip to the center of the plastic zone (i.e., the plastic zone radius). For a material that does not strain harden, the plastic zone radius under these conditions is approximated by the distance ahead of the crack tip in which the elastically calculated stress component acting normal to the crack surface exceeds the yield stress. This is described, for example, in Kanninen and Popelar (1985).

Consider now the case of a flaw contained within a region in which the stresses calculated in the absence of the flaw exceed the yield stress of the material while the surrounding structure remains elastic. Thus the entire system behaves elastically, except for the localized stress concentration region which undergoes plastic strain. In this case, the higher stressed zone is subject to a strain concentration due to "elastic follow-up" of the stiffer or lower stressed regions. Such a strain concentration may exist, for example, at the radius of a fillet or the root of a notch. Under sufficiently high magnitudes of

load, the plastic zone partially or completely envelops the flaw. It is important to distinguish between the localized plastic zone induced by a geometric stress concentrator and the crack-tip plastic zone, which is developed due to the presence of a flaw in an otherwise elastic stress field. A plasticity correction characterized by a crack-tip plastic zone corrected effective crack size applied to an elastic stress intensity factor solution, therefore, is suspect for a flaw that is already embedded in a localized plastic zone. In some cases, however, J integral solutions estimated by calculating the elastic stress intensity factor with a crack-tip plastic zone correction and converting the calculated $K_I$ to J may be reasonably accurate even though the elastically calculated stresses exceed the yield stress. In these cases, the crack is deep enough to relieve the stresses in the stress concentration region sufficiently to focus the plasticity at the crack tip.

Friedman (1999) assessed the adequacy of the crack-tip plastic zone correction for flaws emanating from the root of a notch. The notch geometry represents a typical concave geometric stress concentrator defined by parallel surfaces. Another type of concave geometric stress concentrator is a fillet radius. This geometry, however, is characterized by surfaces perpendicular to each other. A concave stress concentrator, such as a notch, fillet, or circular penetration, differs from a convex concentrator, such as a nozzle corner, in that a tangent plane constructed at a point on the surface lies within the structure for the former, while a tangent plane at a convex surface lies outside the structure. The results reported by Friedman (1999) for flaws at notches and the results of a study carried out for surface flaws at flange fillet radii show that under certain conditions, the crack-tip plastic zone correction is overly conservative. This provides justification for relaxing the correction for surface flaws at locations on a concave geometric stress concentrator and forms the basis for developing general rules for the treatment of plasticity effects for surface flaws at concave stress concentrators.

## CRACK-TIP PLASTIC ZONE CORRECTION TO ELASTIC STRESS INTENSITY FACTOR SOLUTION

In the implicit flaw evaluation procedure of ASME Section XI (ASME, 1998), stress intensity factors are calculated by performing a linear elastic stress analysis without including the flaw in the model. The stress at the flaw location acting through the depth of the flaw is then used to determine the stress intensity factor. The plasticity corrected stress intensity factor is based on the crack-tip plastic zone correction which is embodied in the $K_I$ solution in the form:

$$K_I = \sigma_{eq}\sqrt{\pi a / Q} \tag{1}$$

The flaw shape parameter $Q = \xi_2^2 - q_y$. $\xi_2$ is the complete elliptic integral of the second kind and is approximated in Section XI by $\xi_2 = 1 + 4.593(a/\ell)^{1.65}$, where a and $\ell$ are the flaw depth and length, respectively. $q_y$ is the plastic zone correction given by:

$$q_y = (\sigma_{eq}/\sigma_{ys})^2/6 \tag{2}$$

where $\sigma_{eq}$ is the equivalent crack opening stress and $\sigma_{ys}$ is the material yield strength. The corresponding elastic solution $K_{Ie}$, is given by the same expression with the plastic zone correction removed; thus, $\xi_2^2$ replaces Q in Eq. (1). Q is then expressed in terms of $K_{Ie}$ as:

$$Q = \xi_2^2\left[1 - \frac{1}{6\pi a}\left(\frac{K_{Ie}}{\sigma_{ys}}\right)^2\right] \tag{3}$$

This gives the following for $K_I$ as a function of $K_{Ie}$:

$$K_I = \frac{K_{Ie}}{\left[1 - \frac{1}{6\pi a}\left(\frac{K_{Ie}}{\sigma_{ys}}\right)^2\right]^{0.5}} \tag{4}$$

This expression corresponds to a plastic zone size $a_{pz} = (K_I/\sigma_{ys})^2/6\pi$. Note that the plastic zone corrected $K_I$ is indeterminate if the elastically computed $K_{Ie} \geq \sigma_{ys}\sqrt{6\pi a}$. Consistent with the ASME Section XI plastic zone correction, elastically computed stress intensity factors determined from explicit rather than implicit flaw models can be corrected for plastic zone effects using Eq. (4).

## FLAWS AT NOTCH ROOTS

Fracture evaluations of shallow surface flaws emanating from a notch in a panel subject to tensile loading are directed at assessing flaws in a geometrically concave stress concentration region defined by two parallel surfaces. Figure 1 illustrates the notched panel configuration and geometry. Three sets of two-dimensional elastic and elastic-plastic explicit flaw finite element J integral calculations were performed for various size flaws under plane strain conditions. The results of these calculations were given by Friedman (1999) and are summarized below.

Figure 2 shows plots of $K_I$ vs. flaw depth obtained using (1) the implicit flaw procedure presuming a linearized stress distribution through the flaw depth with no crack-tip plastic zone correction, and (2) a linear elastic explicit flaw finite element analysis. The two curves agree reasonably well, thus providing confidence that the implicit procedure is a reasonable procedure for evaluating stress intensity factors for flaws at notches.

Elastic and deformation theory plasticity calculations were conducted using explicit flaw finite element models. Tensile stresses were applied to the models to assess the ASME Section XI plasticity correction for flaws embedded completely within a localized plastic zone induced by the stress concentrator as well as for flaws penetrating the plastic zone into elastic material. Since applied loads produce higher crack driving forces than equivalent boundary displacements, these calculations were carried out for the limiting case of the applied tensile stress, which also maximizes the effect of plasticity on the crack driving force. J integrals were computed for crack sizes of 0.1, 0.3, and 0.9 inch, and for applied tensile stresses ranging from 5 ksi to 50 ksi.

Plasticity effects are characterized by defining a parameter $K_r = \sqrt{(J_e/J)}$, where $J_e$ and J are the elastically calculated J integral and the J integral computed including deformation theory plasticity modeling, respectively. $K_r$ is an inverse measure of plasticity since lower values of $K_r$ indicate an enhanced plasticity effect. $K_r$

associated with the crack-tip plastic zone correction prescribed in ASME Section XI is given by $K_r = K_{Ic}/K_I$, where $K_I$ is determined as a function of $K_{Ic}$ from Eq. (4). This gives:

$$K_r = \left[1 - \frac{1}{6\pi a}\left(\frac{K_{Ie}}{\sigma_{ys}}\right)^2\right]^{0.5} \quad (5)$$

The plasticity effect embodied in $K_r$ varies with the applied load. The load is also characterized by a dimensionless parameter in order to relate the plasticity correction to the applied load in a general manner. Designating the dimensionless load parameter by $L_r$, curves of $K_r$ vs. $L_r$ can be plotted to define relationships between the effect of plasticity on the crack driving force and the applied loading. Curves of this sort are often designated as failure assessment diagram (FAD) curves since, with the inclusion of information on fracture toughness, they can be utilized to distinguish flaw stability from unstable crack growth. Hong, et al. (1994) used the Central Electricity Generating Board (CEGB) R6 FAD method developed by Ainsworth (1984) to assess flaws in a stress concentration region. In the R6 FAD approach, $L_r$ is defined as the ratio of the applied load to the limit load of the uncracked ligament.

Friedman (1999) presented the results of deformation plasticity calculations based on tensile properties characteristic of both SA-508 Class 2 steel and the higher strength SA-508 Class 4 steel. Using a variation of the FAD approach, the results showed that for all load levels and for relatively shallow flaws with depths up to 0.3 inch, the magnitude of the ASME Section XI crack-tip plastic zone correction is much greater than that of the plasticity correction obtained using explicit flaw finite element J integral results. The plasticity correction is overestimated for these flaw sizes regardless of whether the flaws are completely embedded in the plastic zone induced by the stress concentration or they penetrate the plastic zone into elastic material. (The plastic zone is defined as the region in which the elastically computed von Mises equivalent stress calculated in the absence of the flaw exceeds the yield strength of the material.) For the flaw with depth a = 0.9 inch, on the other hand, the crack-tip plastic zone correction is not overly restrictive for load magnitudes low enough that the flaw penetrates beyond the plastic zone into elastic material. These results demonstrated that the ASME Section XI plasticity correction should be mitigated for flaws of any size provided they are embedded within a localized zone of plasticity induced by the stress concentrator. Therefore, the replacement of the crack-tip plastic zone correction by a plasticity correction described by a less restrictive FAD curve is appropriate for a flaw embedded within the plastic zone existing in the absence of the flaw.

## FLAWS AT FILLET RADII

Relatively shallow surface flaws emanating from flange fillet radii are considered next. The fillet represents a concave stress concentrator defined by perpendicular or nearly perpendicular surfaces (i.e., a 90° included angle). As illustrated in Fig. 3, the flaw is located at a point on the surface of the fillet radius that is defined by an angle of 22.5° from the horizontal and is oriented at the same angle from the horizontal. This location and orientation approximate that of the peak stress and the maximum stress gradient, respectively, from the surface of the fillet radius. A localized plastic zone in which a flaw of up to 0.4 inch in depth is embedded characterizes the stress concentration region. An outer elastic stress field surrounds the plastic zone. Elastic and elastic-plastic J integral finite element analyses were conducted using explicit flaw models for three combinations of fillet radius, R, and flaw depth, a:

R = 1", a = 0.2"
R = 1", a = 0.4"
R = 2", a = 0.4"

The flange is loaded by a uniform pressure acting on the bearing surface as shown in Fig. 3 Linear elastic and elastic-plastic analyses were conducted for each of the three models using the same SA-508 Class 2 and Class 4 material properties employed for the notched panel analysis. Implicit flaw stress intensity factor calculations use the methodology given in Appendix A of ASME Section XI (ASME, 1998). Eq. (4) implements the ASME Section XI crack-tip plastic zone correction.

J integral solutions were determined as functions of applied load for the three explicit flaw finite element models and converted to equivalent stress intensity factors $K_I$ using:

$$K_I = \sqrt{\frac{EJ}{1-\nu^2}} \quad (6)$$

Figure 4 gives plots of the elastically calculated finite element $K_I$ solutions and the corresponding linear elastic implicit flaw solutions. The two solutions agree well for all three combinations of fillet radius and flaw size.

Figure 5 shows plots of the equivalent $K_I$ from Eq. (6) against the applied load obtained from the elastic and deformation plasticity analyses. Figure 5 also plots the plastic zone corrected ASME Section XI $K_I$ solutions for both SA-508 Class 2 and Class 4 materials. The results for the three combinations of fillet radius and flaw depth are qualitatively similar:

1. Inclusion of plasticity in the finite element model increases the crack driving force for load-controlled conditions for which the loading is applied pressure.

2. Plasticity effects are greater for SA-508 Class 2 material than for higher strength Class 4 material.

3. The ASME Section XI plastic zone correction to the $K_I$ solution is overly conservative even for relatively low magnitudes of the applied load.

## FAD BASED PLASTICITY CORRECTION

The previous sections addressed the generation of plasticity corrections for two distinct cases of a geometric stress concentration defined by a concave surface: (1) the stress concentration at the root of a notch defined by two parallel surfaces (included angle of 0°), and (2) the stress concentration at a fillet radius defined by two perpendicular surfaces (included angle of 90°). In both cases, the loading on the uncracked ligament is combined bending and tension. A more general relationship expressed in terms of a FAD curve provides an adequate bound for the two extremes of concave surface geometric stress concentrators. This curve provides a less restrictive plasticity correction for flaws in stress concentration regions.

### FAD Curve Options

The proposed bounding FAD curve is based on one of the three options prescribed in the Level 3 (Advanced) Flaw Assessment

Method developed by the British Central Electricity Generating Board (CEGB) (Ainsworth, 1983), and incorporated into British Standard PD 6493 (1991). The methodology applies to welded structures in general. Stress concentrations due to structural discontinuities are accounted for by calculating peak stresses using appropriate stress concentration factors applied to nominal stresses. Effects of plasticity induced by the stress concentrator and its interaction with the crack are not considered in PD 6493 (1991). The stress concentration correction given by Hong, et al. (1994) is used for this purpose.

The CEGB Level 3 method utilizes a flaw assessment diagram constructed in the form $K_r$ vs. $L_r$, where $K_r = \sqrt{(J_e/J)}$ and $L_r = \sigma_{ref}/\sigma_{ys}$. $\sigma_{ref}$ is a reference stress that, when normalized with respect to the yield stress $\sigma_{ys}$, is equal to the ratio of the applied load to the limit load; i.e., $L_r = \sigma_{ref}/\sigma_{ys} = F/F_o$, where F is a measure of the applied load and $F_o$ is the corresponding limit load. Note that the limit load $F_o$, is associated with the yield stress $\sigma_{ys}$. If the limit load were characterized in terms of the flow stress, which is defined as the average of the yield and ultimate strengths, to accommodate strain hardening, the limit load would be reached at $L_r = 1.30$ for SA-508 Class 2 material or 1.12 for SA-508 Class 2, rather than $L_r = 1.0$.

Three options are given in PD 6493 (1991) for constructing the $K_r$ vs. $L_r$ FAD curve. These options, given in order of increasing complexity, are:

Option 1:

$$K_r = f_1(L_r) = (1-0.14L_r^2)[0.3+0.7\exp(-0.65L_r^6)] \qquad (7)$$

This is a relatively simple relationship that is independent of material properties.

Option 2:

$$K_r = f_2(L_r) = \left[\frac{E\varepsilon_{ref}}{\sigma_{ref}} + \frac{1}{2}\frac{\sigma_{ref}}{E\varepsilon_{ref}}\left(\frac{\sigma_{ref}}{\sigma_{ys}}\right)^2\right]^{0.5} \qquad (8a)$$

$\varepsilon_{ref}$ is related to $\sigma_{ref}$ via the Ramberg-Osgood power law relationship: $\varepsilon_{ref}/\varepsilon_{ys} = \sigma_{ref}/\sigma_{ys} + \alpha(\sigma_{ref}/\sigma_{ys})^n$, where $\varepsilon_{ys} = \sigma_{ys}/E$ and $\alpha$ and n are the power law parameters. Since $L_r = \sigma_{ref}/\sigma_{ys}$, Eq. (8a) can be expressed in terms of $L_r$ as:

$$K_r = f_2(L_r) = \left[\left(1+\alpha L_r^{n-1}\right) + \frac{1}{2}\frac{L_r^2}{\left(1+\alpha L_r^{n-1}\right)}\right]^{-0.5} \qquad (8b)$$

This relationship, which depends on the power law strain hardening parameters of the material, applies to all fracture susceptible materials in general. PD 6493 (1991) gives plots of the Option 2 $K_r$ vs. $L_r$ FAD curve for carbon steel, quenched and tempered steel, and austenitic stainless steel.

Option 3:

$$K_r = f_3(L_r) \qquad (9)$$

$f_3(L_r)$ is determined directly from the results of explicit flaw elastic and elastic-plastic finite element analyses. Therefore, all explicit flaw finite element results correspond to Option 3.

Figure 6 provides plots of the Option 1 FAD curve from Eq. (7) and the Option 2 FAD curves from Eq. (8b) for SA-508 Class 2 and Class 4 materials. The Ramberg-Osgood fitting parameters at 70°F are $\alpha = 2.144$, $n = 6.03$ for Class 2 material and $\alpha = 1.620$, $n = 9.88$ for Class 4. Figure 6 shows that the Option 2 curves give a somewhat greater plasticity effect than the Option 1 curve for $L_r$ values up to about 0.7, which encompasses the expected range of $L_r$ values. The plasticity effect for Class 2 material is greater than that for Class 4 material due to the greater strain hardening capacity of the former.

Plasticity effects may be accommodated by using either the Option 1 or Option 2 methods with calculated values of $K_r$ that are reduced by a stress concentration correction term given by Hong (1994). Comparisons of the Option 3 $K_r = f_3(L_r)$ results obtained from the explicit flaw finite element analyses are made with the following FAD curves:

1. Option 1 $K_r = f_1(L_r)$ FAD curve.
2. Option 1 $K_r = f_1(L_r)$ FAD curve with the stress concentration correction.
3. Option 2 $K_r = f_2(L_r)$ FAD curve.
4. Option 2 $K_r = f_2(L_r)$ FAD curve with the stress concentration correction.
5. Chell modification to Option 2 FAD curve.

The stress concentration correction (Hong, 1994) requires that the $K_r$ vs. $L_r$ curve of either Option 1 or Option 2 be lowered by the quantity $\beta$, which is as follows:

$$\beta = 1.582\,\beta_1\{\exp[-(1-1.25L_r)^2]-0.368\} \qquad L_r \le 0.8 \quad (10a)$$

$$\beta = \beta_1 \qquad L_r > 0.8 \quad (10b)$$

where

$$\beta_1 = 0.0416\,(R/a)^{[0.735-0.0907\ln(R/a)]} \qquad (11)$$

and R/a is the ratio of the local radius of curvature to the flaw depth.

The Chell (1998) modification to the Option 2 FAD curve replaces Eq. (8b) with the following equation for $K_r$:

$$K_r = \left\{\frac{1}{\left[1-\frac{1}{18a\left(1+L_r^2\right)}\left(\frac{n-1}{n+1}\right)\left(\frac{K_{Ie}}{\sigma_y}\right)^2\right]} + \alpha L_r^{n-1}\right\}^{-0.5} \qquad (12)$$

The first term within the brackets { } of Eq. (12) is associated with the classical crack-tip plastic zone correction modified to account for strain hardening, while the second term is associated with the fully plastic J integral solution employed in J-estimation scheme solutions (Chell, 1998). The Chell modification introduces the elastically computed stress intensity factor $K_{Ie}$, as an independent variable needed to determine the plasticity correction $K_r$. This is similar to the plasticity correction given by Eq. (5), but differs from Options 1 and 2 as well as the Hong (1994) correction to Options 1 and 2, which depend only on $L_r$ and, for Option 2, the strain hardening parameters.

## Determination of Reference Stress Parameter $L_r$

A general expression for $L_r$ is developed from the load transmitted across a section that is coplanar with the flaw. The load is expressed in terms of combined membrane and bending loads that act to open the flaw. Assuming that the limit load of the flawed section is attained when that section forms a plastic hinge, the locus of combinations of membrane load $P_o$ and bending load $M_o$ at the limit load condition for a section with a rectangular shape and a thickness h, is given by:

$$M_o/M_{lim} + (P_o/P_{lim})^2 = 1 \qquad (13)$$

$P_{lim} = \sigma_{ys} \cdot h$ and $M_{lim} = \sigma_{ys} \cdot h^2/4$ are the limit loads corresponding to pure membrane load and pure bending load, respectively, across the unflawed ligament. Therefore, $P_o$ and $M_o$ are the "net section" loads. As illustrated in Fig. 8, this limit equation presumes that the presence of a crack-like flaw of depth "a" reduces the load carrying capacity (i.e., the limit load) of the section as if the defect effectively reduced the section thickness from thickness "t" to effective thickness h = t - a.

Conventional stress analyses are conducted in the absence of the flaw; thus, loads transmitted across a section are computed with respect to the "gross section" as if no flaw existed. Letting $P_o^u$ and $M_o^u$ be the gross section membrane load and bending load, respectively, acting across the unflawed section (see Fig. 7) at the limit load condition, $P_o = P_o^u$ and $M_o = M_o^u + P_o^u \cdot a/2$. Letting $\sigma_{Mo} = P_o^u/t$ and $\sigma_{Bo} = 6M_o^u/t^2$, respectively, be the equivalent linear membrane and bending stresses acting across the unflawed section of thickness t, Eq. (13) is used to obtain the following expression for the uniform membrane stress at the limit load condition:

$$\sigma_{Mo} = \frac{\sigma_{ys}}{3}\left[\sqrt{\left(\frac{\sigma_B}{\sigma_M} + 3\frac{a}{t}\right)^2 + 9\left(1 - \frac{a}{t}\right)} - \left(\frac{\sigma_B}{\sigma_M} + 3\frac{a}{t}\right)\right] \qquad (14)$$

$\sigma_B/\sigma_M$ is the ratio of the nominal bending stress to the nominal membrane stress and is presumed to remain fixed during loading to the limit condition.

Eq. (14) has been derived assuming conditions of plane stress. The ASME Section XI procedure presumes plane strain conditions; its plastic zone correction given by Eqs. (2) or (4) likewise applies to plane strain conditions. Therefore, a revision to the limit load equation given above for $\sigma_{Mo}$ is necessary. The flaw configurations under consideration for stress concentration regions are most akin to those for single-edge cracked plates under various combinations of membrane and bending loads. Kumar, et al. (1981) present a number of limit load solutions for edge cracked plates under both plane stress and plane strain conditions. The ratio of the limit load under plane strain conditions to the limit load for plane stress is 1.357 for the single-edge cracked plate under uniform tension, 1.358 for the plate in three-point bending, and 1.359 for the compact tension specimen. The uniformity of these solutions justifies increasing the limit load by a factor of 1.358 for all cases in which flaws exist at a geometric stress concentrator so that, for plane strain conditions,

$$\sigma_{Mo} = 1.358\frac{\sigma_y}{3}\left[\sqrt{\left(\frac{\sigma_B}{\sigma_M} + 3\frac{a}{t}\right)^2 + 9\left(1 - \frac{a}{t}\right)} - \left(\frac{\sigma_B}{\sigma_M} + 3\frac{a}{t}\right)\right] \qquad (15)$$

$L_r$ is therefore given by:

$L_r = \sigma_M/\sigma_{Mo} =$

$$\frac{2.21\,\sigma_M}{\sigma_{ys}} \div \left[\sqrt{\left(\frac{\sigma_B}{\sigma_M} + 3\frac{a}{t}\right)^2 + 9\left(1 - \frac{a}{t}\right)} - \left(\frac{\sigma_B}{\sigma_M} + 3\frac{a}{t}\right)\right] \qquad (16)$$

$\sigma_M$ is the membrane stress applied across the gross section. $\sigma_M$ and $\sigma_B$ differ from $\sigma_m$ and $\sigma_b$ defined in Appendix A to ASME Section XI as the equivalent membrane and bending stresses acting over the depth of the flaw. The latter are used to evaluate stress intensity factors from stress distributions linearized over the flaw depth. Eq. (15) shows that the membrane stress at the limit load condition decreases with increasing flaw size.

For the notched panel shown in Fig. 1, $\sigma_B/\sigma_M = 2$ and t = 3". For the flange fillet radius illustrated in Fig. 3, $\sigma_B/\sigma_M = 4.126$ and t = 14.69" for fillet radius R = 1", and $\sigma_B/\sigma_M = 4.306$ and t = 14.78" for fillet radius R = 2". With this information, the Option 1 and Option 2 FAD curves plotted in Fig. 6 and their modifications to accommodate cracks in stress concentration regions are constructed and compared with the corresponding Option 3 FAD curves obtained directly from finite element solutions.

## Plasticity Correction for Flaws in Notched Panel

Figures 8-10 show plots of the Option 1, Option 2, and Option 3 (explicit flaw finite element analysis) FAD curves for the notched panel with flaw depths 0.1 inch, 0.3 inch, and 0.9 inch, respectively, for both SA-508, Class 2 and Class 4 materials. These figures also include plots of the corresponding ASME Section XI crack-tip plastic zone correction (PZC) FAD curve for which $K_r$ is calculated from Eq. (5) as well as the Chell modified Option 2 FAD curve. Figures 8 and 9 apply to relatively shallow flaws. They show that except for very low values of $L_r$ for which the loading magnitude is small enough that the flaw is not embedded in a plastic zone, the crack-tip plastic zone correction in the ASME Section XI brittle fracture evaluation procedure significantly overestimates the plasticity effects. The deeper 0.9 inch flaw extends beyond the localized plastic zone into elastic material. Figure 10 shows that the ASME Section XI plastic zone correction provides a very good estimate of the plasticity effect for SA-508, Class 2 material, while it underestimates the plasticity effect somewhat for Class 4 material.

Figure 8 shows that neither the Option 1 nor Option 2 FAD curves bound the Option 3 explicit flaw finite element plasticity correction FAD curve for a very shallow flaw. For the deeper 0.3-inch flaw, Fig. 9 shows that the Option 2 curve provides a lower bound, but the Option 1 curve is unconservative. For the 0.9-inch deep flaw that extends into elastic material, both the Option 1 and Option 2 curves lower bound the Option 3 curve, but are more restrictive than the ASME Section XI plastic zone correction.

The Option 1 and Option 2 FAD curves adjusted for the stress concentration using the correction terms of Eqs. (10) and (11) lower bound the plasticity effect at all load levels, although they become increasingly conservative at higher load levels. Since the Option 1 corrected curve is less restrictive than the Option 2 corrected curve and is simpler to implement because it does not depend on material properties, Option 1 is preferred.

The Chell modification to the Option 2 FAD curve as given by Eq. (12) also gives a reasonably conservative estimate of the plasticity correction for the shallower flaw depths of 0.1 inch and 0.3 inch for which the flaws are embedded in a plastic zone. Since the Chell model was developed specifically for flaws at notches, this result is not surprising. Figure 10 shows, however, that the Chell modification slightly underpredicts the plasticity correction for the 0.9-inch flaw at relatively low load levels.

### Plasticity Correction for Flaws at Flange Fillet Radius

Figures 11-13 show plots of the Option 1, Option 2, and Option 3 FAD curves for flaws located at fillet radii. In all cases, the ASME Section XI plastic zone correction is overly conservative. The Option 1 and Option 2 curves bound the Option 3 explicit flaw finite element curves for relatively large values of the loading parameter $L_r$, but underestimate the plasticity effect for lower magnitudes of load. The Option 1 curve corrected for the stress concentration provides a reasonably conservative estimate of the plasticity effect for all levels of $L_r$. The Chell modification of the Option 2 FAD curve, on the other hand, is somewhat of an improvement over the ASME Section XI correction; however, it is overly conservative in all cases.

The Option 3 explicit flaw finite element FAD curve depends on the strain hardening characteristics of the material. The Option 3 curves of Figs. 11-13 show that except for low values of $L_r$, the plasticity correction is more pronounced for SA-508 Class 2 material than for the higher strength Class 4 material. However, the differences are small enough that separate bounding FAD curves that distinguish between the two materials are not warranted.

### Summary

The results plotted in Figs. 8-13 show that the Option 1 FAD curve adjusted for stress concentration effects by the correction given by Eqs. (10) and (11) provides a satisfactory bound to the stress intensity factor plasticity correction for all cases at all load levels. Note that the ASME Section XI plastic zone correction is appropriate for flaw depths and load levels for which cracks penetrate the plastic region and extend into elastic material. However, the corrected Option 1 curve can still be used since in all cases it provides a conservative bound to the Option 3 explicit flaw curve.

## CONCLUSIONS

The results of explicit flaw finite element calculations for defects located within localized regions of plasticity lead to the following conclusions:

1. Elastic implicit flaw ASME Section XI stress intensity factor solutions for flaws in stress concentration regions are reasonably conservative estimates of the linear elastic stress intensity factor. Plasticity corrections developed from explicit flaw finite element analyses applied to the ASME Section XI solution should yield plasticity corrected stress intensity factor solutions that also are reasonably conservative.

2. The crack-tip plastic zone correction in the ASME Section XI flaw evaluation procedure overestimates plasticity effects for flaws embedded in localized stress concentration regions in which the elastically computed von Mises stress exceeds the material yield strength. This results from stress intensity factor solutions that are based on the elevated stresses in the stress concentration region containing the flaw, but that account directly for neither the geometry of the region nor the presence of a zone of localized plasticity induced by the stress concentrator. The ASME Section XI plasticity correction, however, is appropriate and not overly restrictive if the flaw size and the magnitude of loading are such that the defect penetrates the plasticity region and extends into elastic material.

3. A generalized plasticity correction to an elastically computed stress intensity factor solution is defined using a failure assessment diagram (FAD) curve. The FAD curve graphically depicts the plasticity effect as a function of the applied load normalized with respect to the limit load of the section containing the flaw. The enhancement of the crack driving force due to plasticity is estimated conservatively by a FAD curve obtained from Option 1 of the Level 3 CEGB flaw assessment method. The curve is corrected for stress concentration effects by a term that is a function of both the applied load and the ratio of the local radius of curvature to the flaw depth. The bounding Option 1 FAD curve, which in general is much less restrictive than the ASME Section XI plastic zone correction for flaws embedded in plastic zones, is independent of material properties.

4. Plasticity effects increase the crack driving force for conditions of applied loading. A plasticity correction to the linear elastically computed stress intensity factor solution should, therefore, be included in fracture evaluations of components subject to such loading. The Option 1 plasticity correction accommodates different material yield strengths through the normalized applied load which is inversely proportional to the yield strength so that the plasticity effect is greater for lower strength materials. This allows the correction to be expressed in terms of a FAD curve applicable to all materials.

## REFERENCES


Ainsworth, R. A., 1984, "The Assessment of Defects in Structures of Strain Hardening Material," Engr. Fracture Mech., Vol. 19, No. 4, pp. 633-642.

ASME Boiler & Pressure Vessel Code, 1998, Section XI, Rules for Inservice Inspection of Nuclear Power Plant Components, Appendix A, pp. 401-422.

Chell, G. G., 1999, "A J Estimation Scheme for Cracks at Notches," Appendix D to Development of a Practical Methodology for Elastic-Plastic and Fully Plastic Fatigue Crack Growth, NASA/CR-1999-209428.

Friedman, E., 1999, "Assessment of Cracks in Stress Concentration Regions With Localized Plastic Zones," Computer Technology, ASME PVP-Vol. 385, pp. 279-286.

Hong, Q., Ying, T., and Liankui, S., 1994, "The Assessment of Flaws in a High Stress Concentration Region," Intl. J. Pres. Ves. & Piping, Vol. 57, pp. 201-206.

Kanninen, M. F., and Popelar, C. H., 1985, Advanced Fracture Mechanics, Oxford University Press, New York, p. 172.

Kumar, V., German, M. D., and Shih, C. F., 1981, "An Engineering Approach for Elastic-Plastic Fracture Analysis," EPRI NP-1931, Project 1237-1.

PD 6493, 1991, Guidance on Methods for Assessing the Acceptability of Flaws in Fusion Welded Structures, British Standards Institution, London.

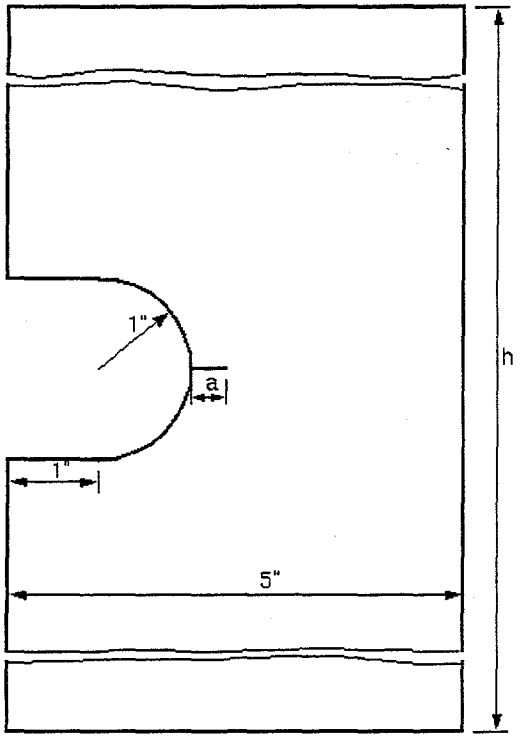


**Figure 1. Notched Panel Geometry**

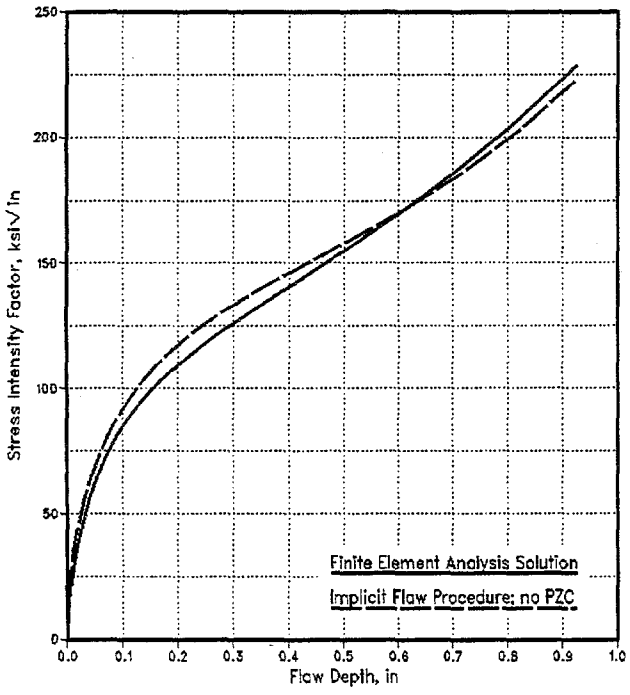


**Figure 2. Elastic Stress Intensity Factor vs. Flaw Depth for Notched Panel; Applied Tensile Stress = 20 ksi**

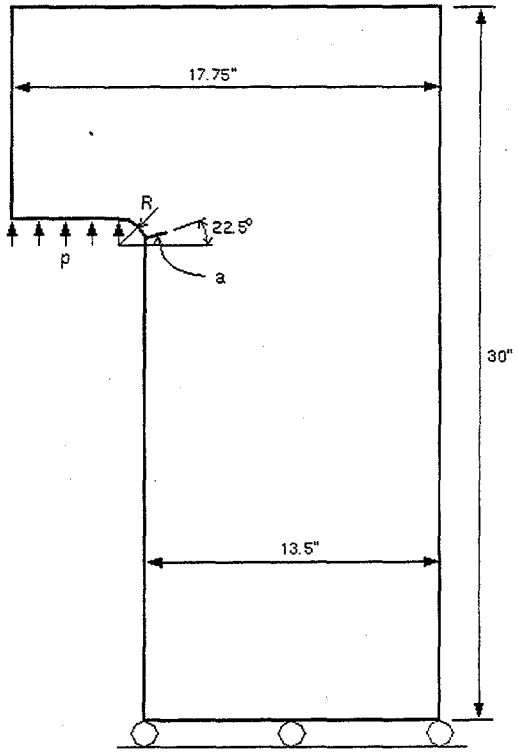


**Figure 3. Flange With Flaw at Fillet Radius**

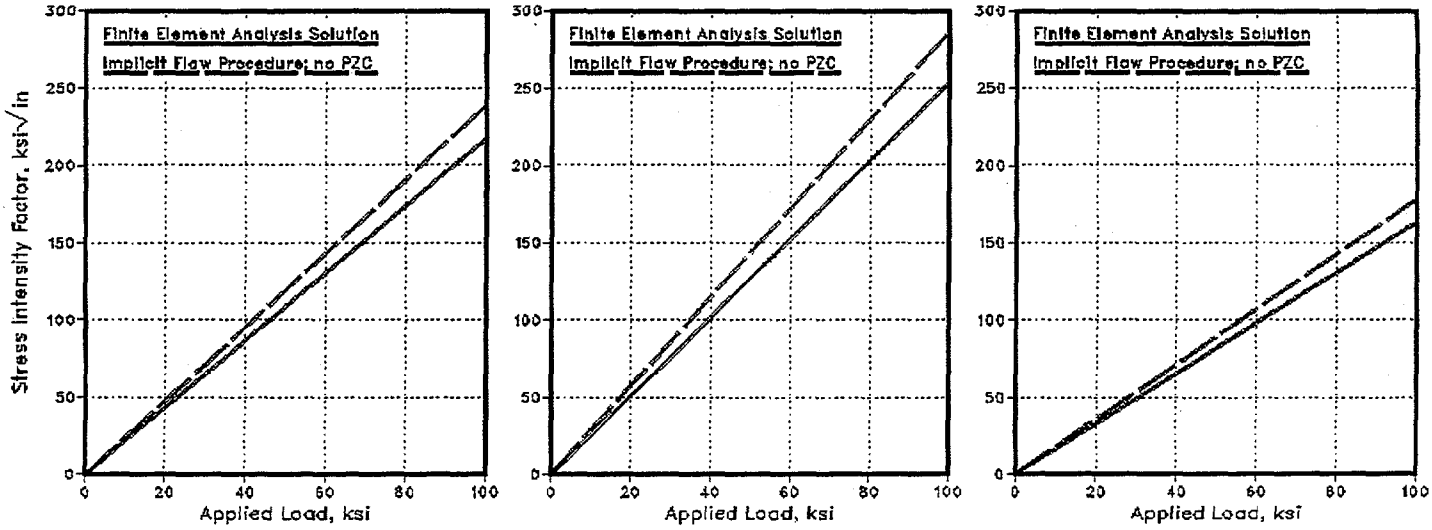


(a) Fillet Radius = 1", Flow Depth = 0.2" (b) Fillet Radius = 1", Flow Depth = 0.4" (c) Fillet Radius = 2", Flow Depth = 0.4"

**Figure 4. Elastic Stress Intensity Factor Solutions for Flaw at Fillet Radius**

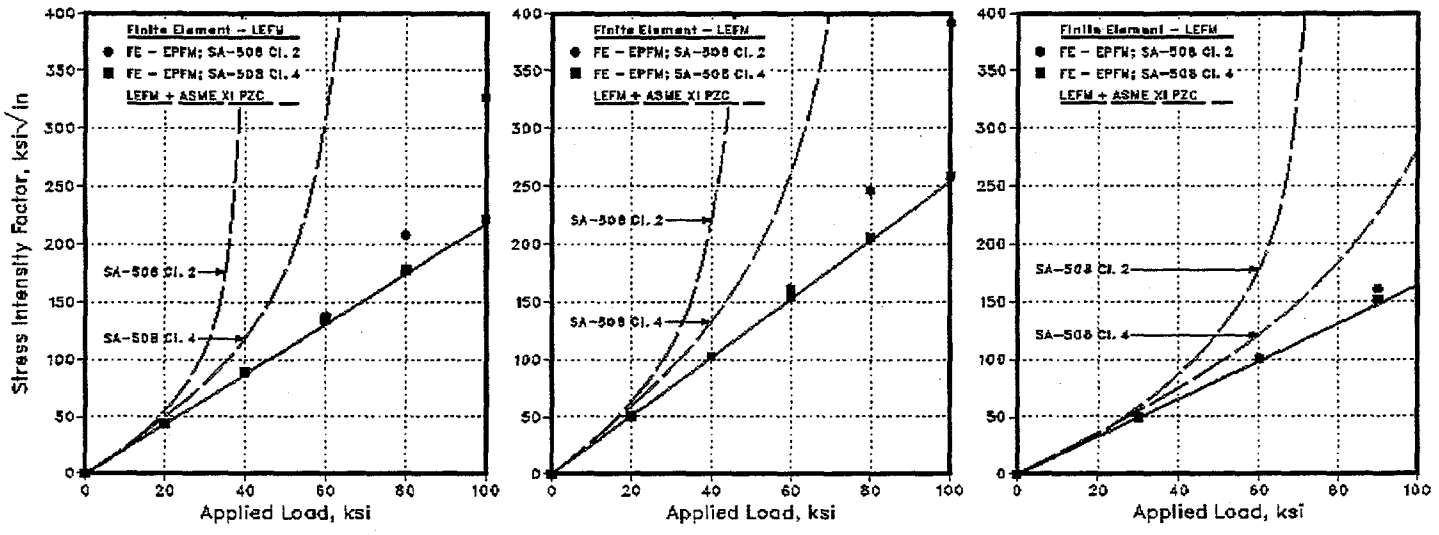


(a) Fillet Radius = 1", Flow Depth = 0.2" (b) Fillet Radius = 1", Flow Depth = 0.4" (c) Fillet Radius = 2", Flow Depth = 0.4"

**Figure 5. Stress Intensity Factor vs. Applied Load at Fillet; LEFM and EPFM Solutions and Comparison With Plastic Zone Corrected Solutions**

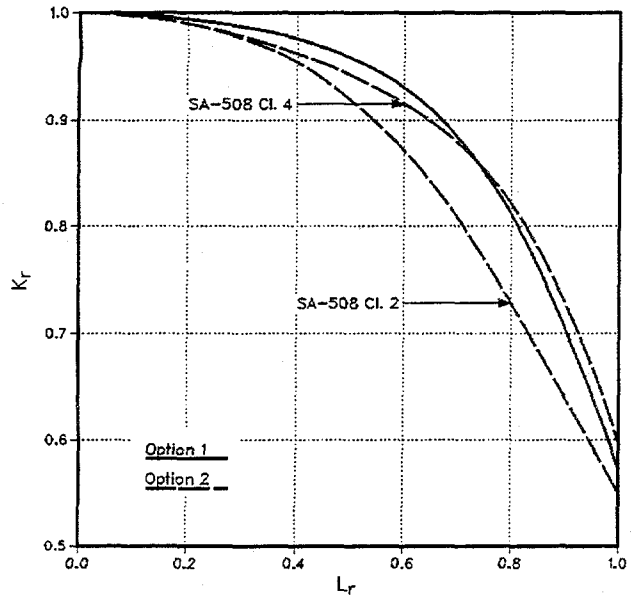


**Figure 6. CEGB Level 3 Option 1 and Option 2 FAD Curves**

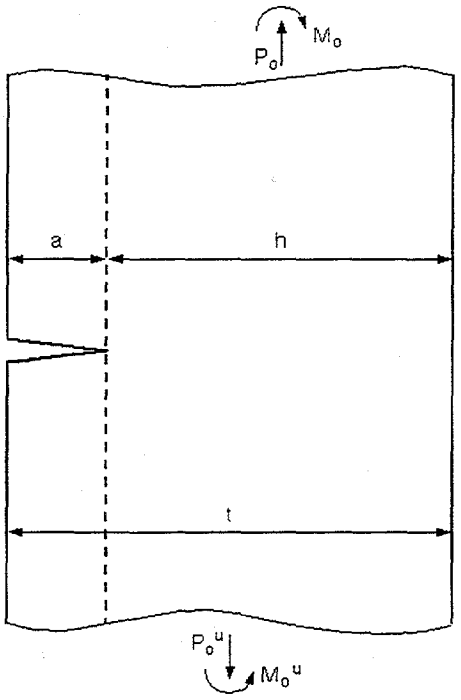


**Figure 7. Loading on Flawed and Unflawed Section**

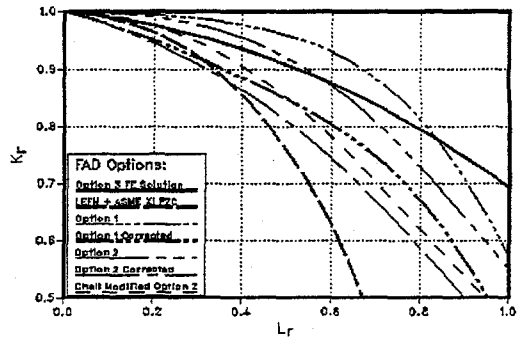


(a) SA–508 Class 2

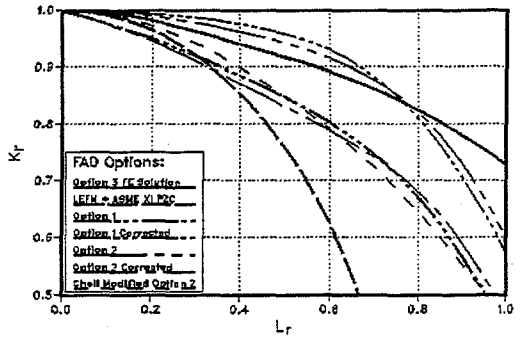


(b) SA–508 Class 4

**Figure 8. FAD Curves for Flaw at Notch a = 0.1 inch**

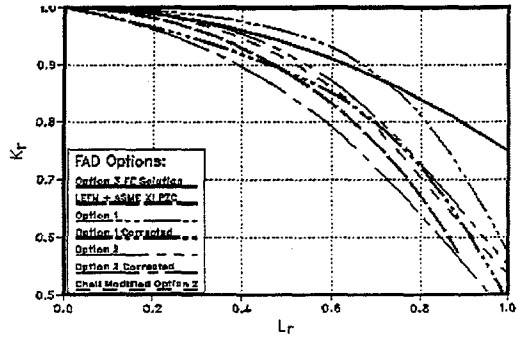


(a) SA–508 Class 2

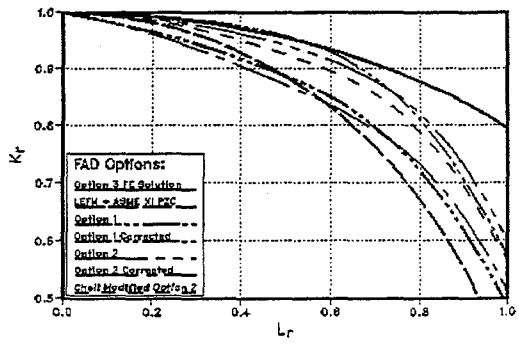


(b) SA–508 Class 4

**Figure 9. FAD Curves for Flaw at Notch a = 0.3 inch**

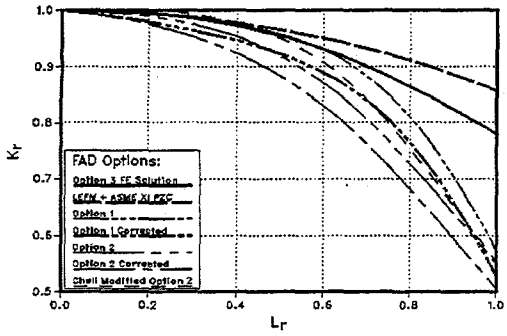


(a) SA–508 Class 2

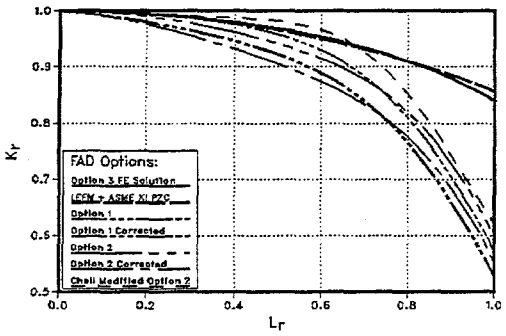


(b) SA–508 Class 4

**Figure 10. FAD Curves for Flaw at Notch a = 0.9 inch**

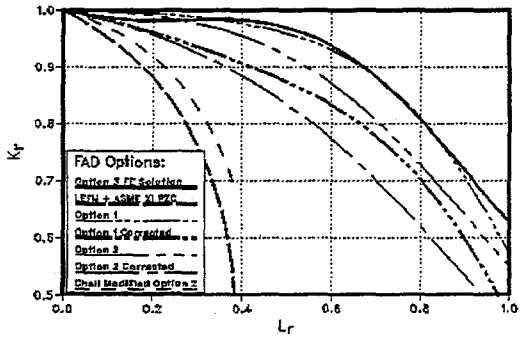


(a) SA–508 Class 2

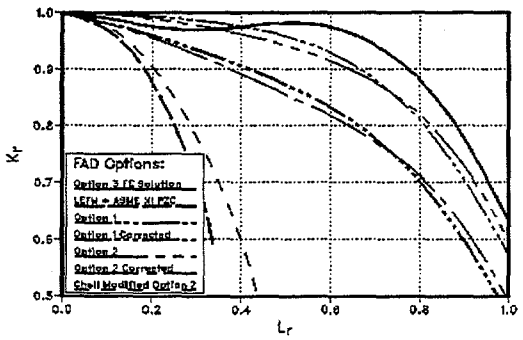


(b) SA–508 Class 4

**Figure 11. FAD Curves for Flaw at Fillet Radius R = 1 inch, a = 0.2 inch**

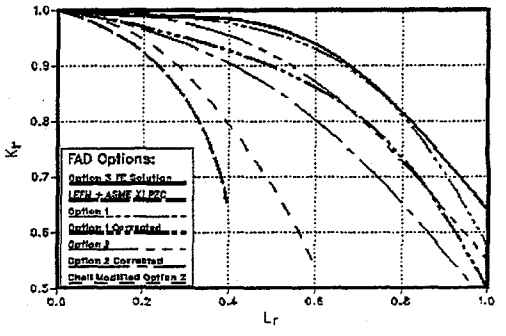


(a) SA–508 Class 2

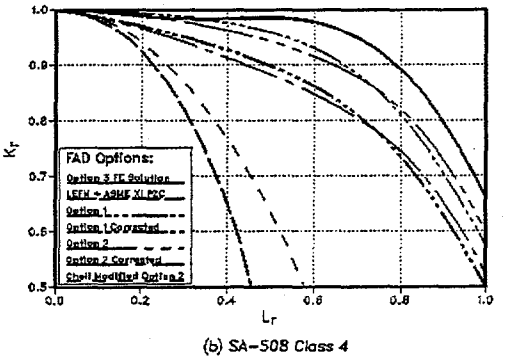


(b) SA–508 Class 4

**Figure 12. FAD Curves for Flaw at Fillet Radius R = 1 inch, a = 0.4 inch**

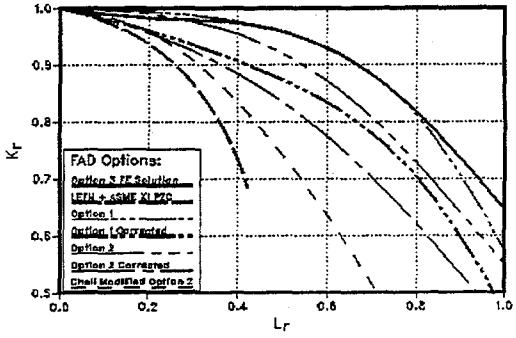


(a) SA–508 Class 2

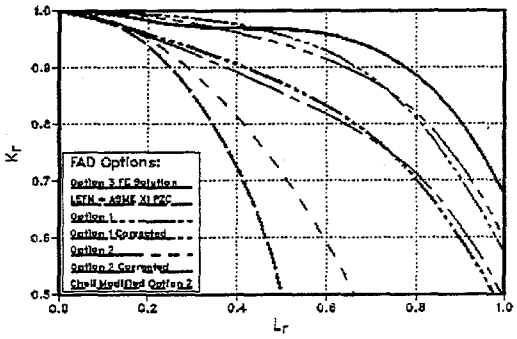


(b) SA–508 Class 4

**Figure 13. FAD Curves for Flaw at Fillet Radius R = 2 inches, a = 0.4 inch**